CHARACTERISTICS OF BOSE GLASS IN A DISORDERED OPTICAL LATTICE

HONORS THESIS

Presented to the Honors Committee of
Texas State University
in Partial Fulfillment
of the Requirements

for Graduation in the Honors College

by

Adam Anthony Chalupa

San Marcos, Texas
December 2014

CHARACTERISTICS OF BOSE GLASS IN A DISORDERED OPTICAL LATTICE

Thesis Supervisor:

_____

Byounghak Lee, Ph.D.
Department of Physics

Approved:

_____

Heather C. Galloway, Ph.D.
Dean, Honors College

ACKNOWLEDGEMENTS

I would like to thank my thesis advisor, Dr. Byounghak Lee, for his knowledge and patience through the writing and work done to produce this thesis. I have been working with him since my start in the Department of Physics at Texas State, and among many different things he has taught me, the most important have been to think before I speak and analyze before I opinionate. I would like to thank my wife, Leta Chalupa, who has been exceptionally supportive and has never ceased to give me wise advice. I would also like to thank my two friends and colleagues in the physics department, Eric Welch and Aureliano Perez, for their collaboration, knowledge, and encouragement.

TABLE OF CONTENTS

ABSTRACT

When bosonic atoms are trapped in optical lattices, they exhibit one of the two phases: superfluid (SF), where atoms move coherently without any collisions, or Mott insulator (MI), where atoms are localized. These quantum phases on clean bosonic lattices have been thoroughly studied [7,8,13]. When the optical lattices are disturbed by a source of disorder, a third exotic phase, Bose glass, has been predicted to appear [1,3]. In this thesis, we utilize a mean field theory coupled within the Bose Hubbard model [1] to investigate the phases of two-dimensional disordered bosonic optical lattices. We study the phase of the systems as a function of chemical potential and hopping-parameter by using the SF density, compressibility, and number density of the system as characterizing order parameters. We have discovered that, even with the presence of disorder, the phase at each optical lattice site is either MI or SF. Real-space analyses show that the disordered systems contain separated MI and SF phases at different sites, rather than a new global phase. We have also discovered that the local phase at each lattice site is weakly correlated with the phase of neighboring sites; the phase at each site strongly depends on the strength of the local disorder potential.

Chapter 1. INTRODUCTION

At very low temperatures, where the kinetic energy of atoms is small, atoms can be trapped by optical potentials made of laser lights shined in opposite directions. When multiple lasers are crossed in a periodic manner, the optical traps form a lattice, which resembles a perfect crystal lattice. Bosons are particles of particular interest because they are not subject to the Pauli Exclusion Principle, which prohibits atoms from having the same quantum state with one another [2]. When trapped in such perfect lattices are in one of two 'phases': they either do not move at all, a Mott insulator (MI) phase, or move freely without collision, a superfluid (SF) phase [8,13]. With trapped bosons at very low temperatures, large scale observations of their quantum behavior can be seen as they drop into what is called a Bose Einstein Condensate [13]. When a lattice is disordered by something such as an optical speckle field [5,6,10], a third phase called "Bose glass" (BG) has been predicted to appear. This phase is supposed to show up between the Mott insulating and SF phases and is described as a compressible non-superfluid phase [1,3,11]. Since the observation of the Bose-Einstein condensate [13], many different studies to characterize these phases in both clean and disordered lattices have been done [3,5,6,9,10].

In this thesis, we utilize the Bose Hubbard model to theoretically study what happens when bosons are trapped in disordered optical lattices. We define order parameters that distinctly characterize MI, SF, and BG, and analyze how the order parameters change as a function of system parameters. In particular, we investigate the local properties of the BG phase and study if the local MI to SF phase transition happens directly between them or indirectly via the BG phase.

Our study differs from previous studies in that our system size is very large and we focus on the local site characteristics rather than the averaged global system-wise characteristics.

Chapter 2. MODELS AND CALCULATION METHODS

2.1 THE BOSE HUBBARD MODEL

We describe the energy of two-dimensional optical lattices with bosonic atoms using a Bose Hubbard Hamiltonian [1]:

$$H_{BHH} = -\sum_{\langle i,j \rangle} t_{ij} a_i^\dagger a_j + \frac{U}{2}\sum_i n_i(n_i+1) - \mu \sum_i n_i + \sum_i V_i n_i \quad (1)$$

In this model the energy of the system is described by: 1) hopping energy: $-\sum_{\langle i,j \rangle} t_{ij} a_i^\dagger a_j$, t_{ij}, associated with atoms moving from one lattice site to nearest neighboring sites, 2) the on-site interaction energy: $\frac{U}{2}\sum_i n_i(n_i+1)$, which is the energy cost to put more than one atom at the same site, 3) the chemical potential: $-\mu \sum_i n_i$, the energy that controls the number of atoms of the system, and 4) the random disorder potential: $\sum_i V_i n_i$, which changes the depth of optical lattice sites randomly. Different values of (*t, U, V*) combinations correspond to different systems. The energy operator, the Hamiltonian, is written in a site-dependent number state basis. The state at each site is a linear combination of the number states. In Eq. (1) each *i* stands for a site index in the system. $a_i^\dagger a_i$ is the boson creation (annihilation) operator at site *i*, $-t_{ij}$ is the hopping matrix element associated with the energy moving from sites *j* to site *i*, $\hat{n}_i = a_i^\dagger a_j$ is the number operator, *U* is the on-site interaction energy, μ is the chemical potential, and V_i is

the disorder potential. In a clean system, V_i is zero for every site. To change the optical lattice's phase, we alter the following energy parameters: 1) $t = t_{ij}$*:* the hopping parameter, 2) *U:* the on-site potential, and 3) *V:* the disorder potential. Changes in these parameters correspond to systems with different trap potentials and particle numbers.

Figure 2.1 is a pictorial description of the Hamiltonian operator in Eq. (1).

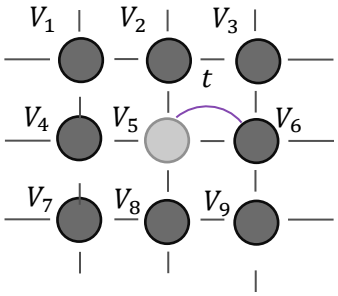

Fig. 2.1: Cartoon depicting the Bose-Hubbard Hamiltonian. When the system becomes disordered, then the depth of each site changes (*V*). In a clean system, all values of V_i would be the same, i.e. $V_1 = V_2 = \cdots = V_N$.

2.2 Mean Field Theory

There are several different techniques that have been used for trapped bosons in optical lattice calculations. Popular calculation techniques include the Monte Carlo method, Gutzwiller Approach and Mean Field Theory [3,8,9]. Taking into account all "many-body" interactions in every site is impractical because the computational cost to find the solution for such a Hamiltonian increases exponentially. For example, if we have *M* number of states at each site in a *N*-site lattice, the diagonalization of the Hamiltonian matrix will need approximately M^{3N} number of algebraic operations. For a system we study in this these, *M =15* and $N = 10^4$, and the solution would require $15^{30,000} \approx 10^{35,000}$ numerical operators. Even with the fastest supercomputer of this present day

which does around 10^{12} operations per second, the computation would take $10^{34,982} seconds \approx 10^{34,975} years$.

As a practical alternative, we employ a mean-field approximation. Within this method, we map a many-site problem to a single-site problem by approximating the creation (annihilation) operators at neighboring sites to superfluid density (complex conjugate of superfluid density). For site *i,* the hopping term in Equation 1 is approximated as:

$$a_i^\dagger a_j \approx a_i^\dagger \langle a_j \rangle + \langle a_j^\dagger \rangle a_i - \langle a_i^\dagger \rangle \langle a_j \rangle \qquad (2)$$

This results in a modification of the Hamiltonian in Equation 1 as:

$$H_{BHH(2)} = \sum_i h_i \qquad (3)$$

$$where\ h_i = -t\left(a_i^\dagger \langle a_j \rangle + \langle a_j^\dagger \rangle a_i\right) + \frac{U}{2} n_i (n_i + 1) + (V_i - \mu) n_i \qquad (4)$$

The term h_i is the single site Hamiltonian operator. States at different sites are related only through the expectation value of the creation and annihilation operators.

We try to find the solution of Eq. (3) numerically. Since each site is independent of each other, instead of solving an eigenvalue equation for the total Hamiltonian H_{BHH}, we solve the eigenvalue problem for h_i one site at a time. The total solution of $H_{BHH(2)}$ is a product of solutions of h_i. In actual numerical procedures, we start from a randomly guessed solution at each site. We span the whole lattice site-by-site and solve for h_i. The number of operations to solve each h_i is of order M^3. We found that *M=15* gives a good

convergence. The computational cost for a site Hamiltonian is, therefore, only $15^3 = 3375$ operations. While we move from one site to a neighboring site, we use the solution from the previous site to update the mean-fields, *i.e.* the expectation values $\langle a_i \rangle$ and $\langle a_i^\dagger \rangle$. After each iteration we check if the output mean-fields are the same as the input mean-fields. If they are not the same, we update the mean-fields using the mean-fields from the previous iteration and use them as new inputs for the next iteration. We continue this procedure until we achieve a self-consistency within the mean fields, and the input and output mean-fields become identical.

2.3 Order Parameters

We characterize the phase of any optical lattice's using a combination of three order parameters:

1. Compressibility (κ): The rate change of particle number when chemical potential is changed.
2. SF Density (ψ): The measure of SF in a system.
3. Number Density (n): The number of atoms.

In the MI phase, the SF density is zero, the compressibility is zero, and number density is an integer [3]. In the SF phase, the SF density and compressibility are non-zero, and the number density is not necessarily an integer [3,11]. Finally, the Bose glass phase has zero SF density, but non-zero number density and compressibility.

Within our mean-field theory the above order parameters are defined as:

$$\bar{\kappa} = \frac{1}{N}\sum_i \kappa_i = \frac{1}{N}\sum_i (\langle \hat{n}_i^2 \rangle - \langle \hat{n}_i \rangle^2) \qquad (5)$$

$$\bar{\psi} = \frac{1}{N}\sum_i \psi_i = \sum_i \langle a_i \rangle \qquad (6)$$

$$\bar{n} = \frac{1}{N}\sum_i \langle \hat{n}_i \rangle = \sum_i \langle a_i^\dagger a_i \rangle \qquad (7)$$

In Equations 5-7, N is the number of sites.

In what follows, we study how the complexity of the disorder configurations influences the phase of the lattice. For this purpose, we start with a simple disorder configuration where binary values of disorder potentials are randomly assigned at different sites (See the left figure in Figure 2.2). We increase the complexity to ternary (three different disorder potential values), quaternary, etc. The right figure in Figure 2.2 shows a uniform disorder configuration where disorder potential of uniformly spaced values within $(-\frac{\Delta}{2}, \frac{\Delta}{2})$ are randomly distributed in real space.

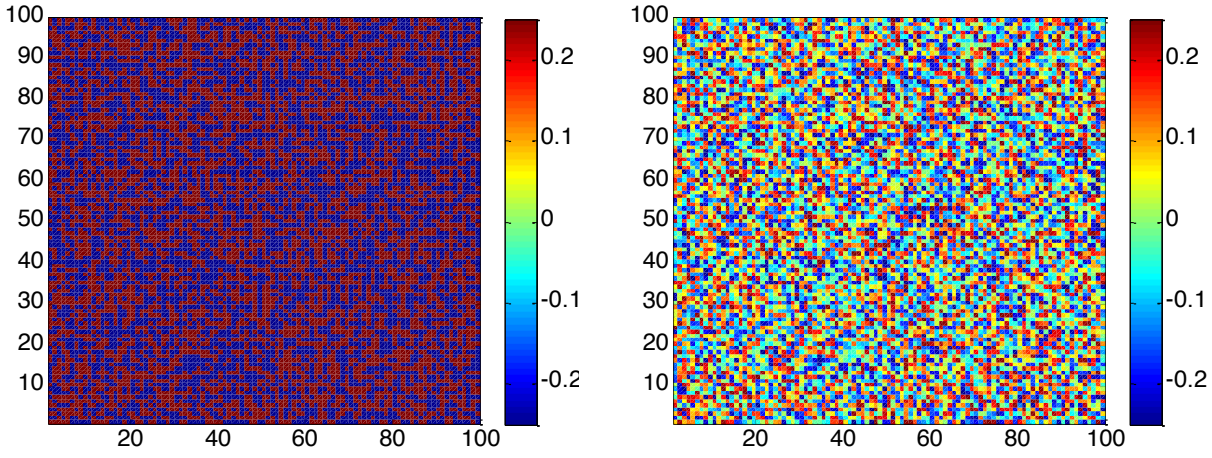

Fig 2.2: Two disorder potential maps used to simulate an optical speckle field scattered across a lattice. The left is a map of binary disorder (two different divisions) and (b) is of 200 different divisions (essentially uniform disorder). The maximum and minimum disorder strength is the same across both, the only difference is the possible amount of different potentials within that range.

In the third chapter, we create quantum phase diagrams to help us predict the quantum phase of a system through the deviation of chemical potential (μ) and lattice kinetic energy (t). The phase diagram helps us understand how the system's phase changes as a function of chemical potential and the hopping parameter. In each different regions of the phase diagram, or phase space, the relationship of the system's phase between these two values can be observed.

For certain figures we utilize a "Phase Boundary" algorithm, which allows us to characterize where the system goes from zero to non-zero values in the quantum phase diagrams. This ensures simplicity when looking for phase transitions:

$$C_{i,j} = \begin{cases} 0 \; if \; \kappa, \Psi < 10^{-4} \\ 1 \; for \; \kappa, \Psi \geq 10^{-4} \end{cases} \qquad (8)$$

At each site $C_{i,j}$ in a parameter phase diagram that is of *i x j* size for phase parameters SF density, Ψ, and compressibility, κ.

Chapter 3. PHASE CHARACTERIZATION

3.1 CLEAN SYSTEM PHASE DIAGRAMS

In this section, we study how the phase of clean systems changes as a function of the system's energy parameters. The independent parameters are the hopping parameter (t) and the chemical potential (μ). The phase of the system is determined by the order parameters, κ, ψ, and n, as discussed in Chapter 2. The vertical axis of these diagrams is μ/U and the horizontal is t/U. Because the repulsive on-site interaction is usually larger than the hopping parameter, we limit our calculations within a small range of t/U. Fig 3.1 shows that, for a given chemical potential, the systems are MI for small hopping parameters (inside the blue lobes) and that the phase changes to SF at larger hopping parameters (outside the lobes). In the MI lobes, the number density is fixed integer values, the compressibility is zero and there is no SF density. Moving up the μ axis, the system number density increments by one in each separate lobe and the actual shapes shorten in length and remain constant in height [14]. Note that the transition from MI to SF is direct, there is no other phase between them.

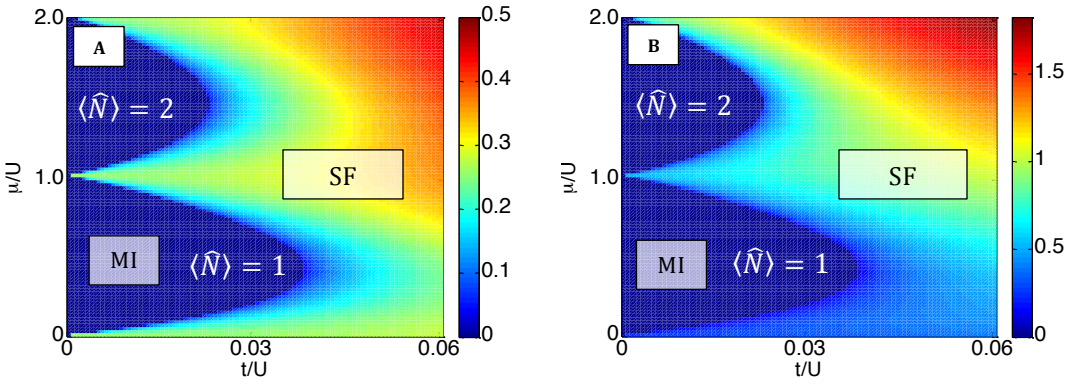

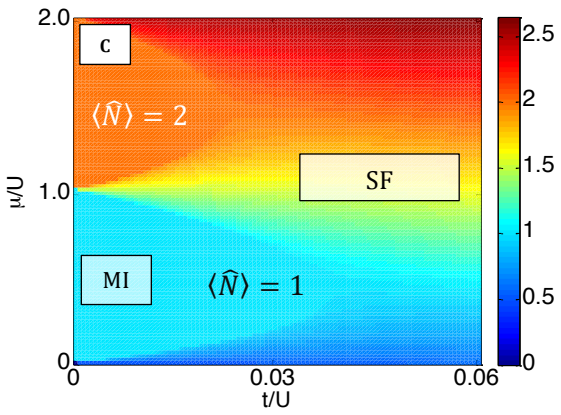

FIG. 3.1 Parameter quantum phase diagrams giving statistical averages over clean real space lattices for values of compressibility (A), SF Density (B), and Normal Density (C). At each point in each chart, we can predict the quantum phase of a real system in accordance to the parameters discussed in 2.2. When any disorder is introduced, it is predicted that there is a region of Bose glass which arises from the boundaries of the lobes, reducing their areas and growing larger as the disorder strength increases [1].

3.2 The Number Density and Compressibility Relationship

We have discovered that the paired compressibility (κ) and number density (n) values for sites in a disordered system against those of multiple clean systems are very similar. When looking at the compressibility of a clean system and comparing it to a single site with the same compressibility value in a dirty lattice, they both share the same number density value as well. This implies that each site in a disordered system does not really care about the phases of sites around it, or they are weakly correlated between one another. The relationship between κ and n is shown in Fig 3.2 and Fig 3.3. These are density plots that vary in color according to the amount of sites (Fig. 3.2 *a*) or clean systems (Fig. 3.2 *b*) that have a particular κ and n value.

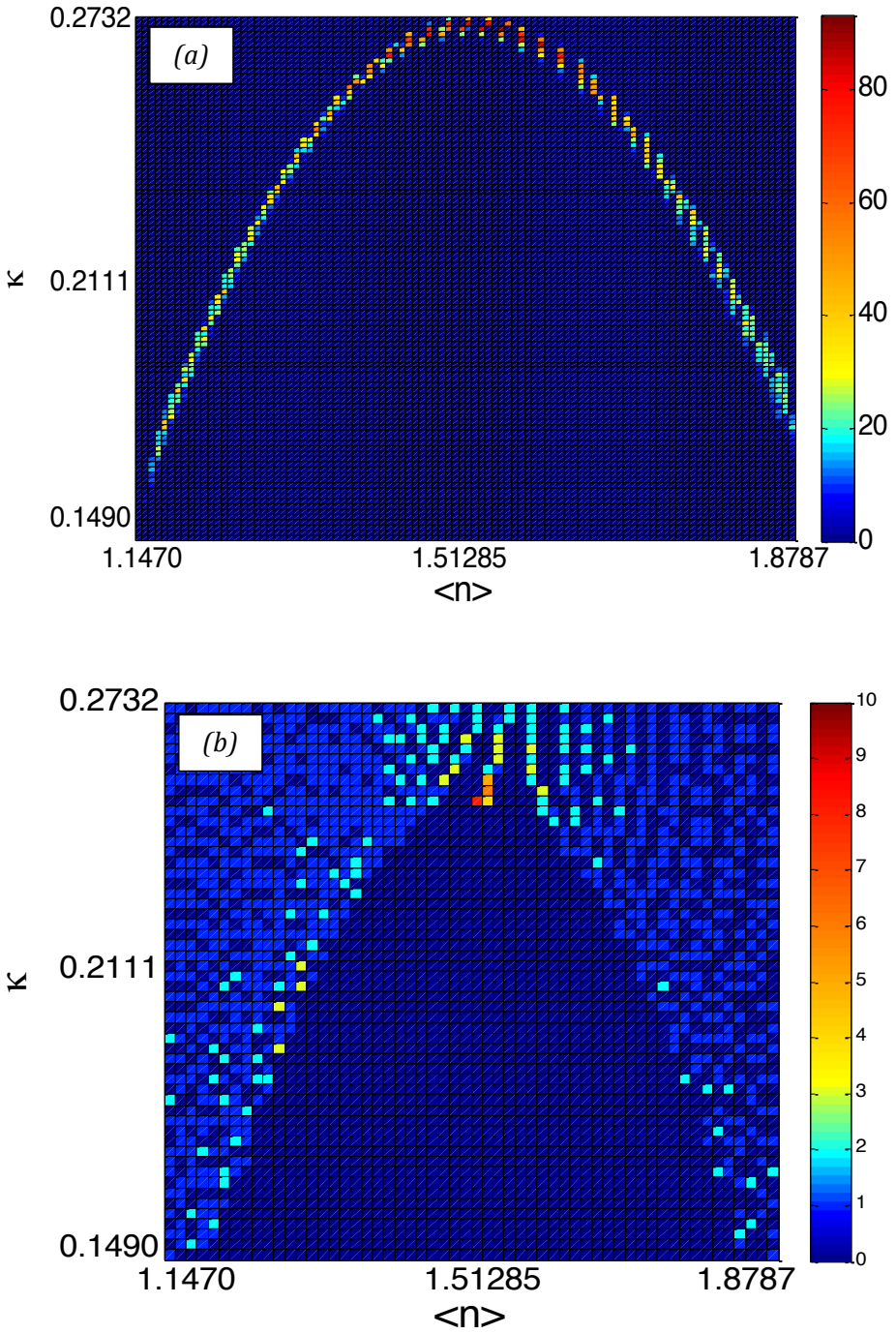

Figure 3.2: Density maps of lattice sites that correspond with a certain number density and compressibility value ($< n >, \kappa$). Diagram *a* is counted over a single disordered lattice with a system chemical potential of $\mu/U = 1.0$ and $t/U = 0.0255$ or point (1.0,

0.0255) in Figure 3.12. Diagram *b* was created through the density plot of compressibility and number density through a clean phase diagram.

In Figure 3.2, the top figure *(a)* shows the compressibility and number density relationship between all sites in a disordered system as a density plot. The differences in color show the population of (κ, n) pairs. The lower figure, *b,* shows a very similar plot crafted from clean system κ and n values which correspond to the clean compressibility and number density diagrams. The relationship between the two is apparent, and since they are remarkably similar we can craft a new means of generating any disordered phase diagram. Figure 3.3 shows the relationship between κ and n in clean systems. In Figure 3.3, we show where Figure 3.2 *b* came from. Again, the color map corresponds to the population (likelihood) of the (κ, n) pairs.

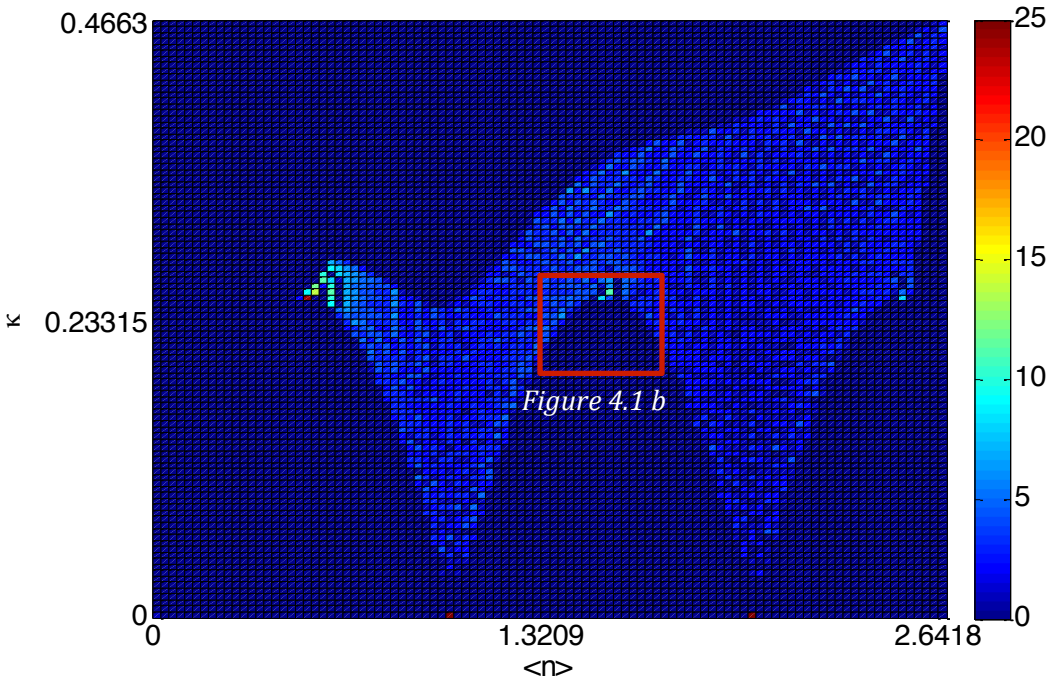

Figure 4.1 b

Figure 3.3: A density point plot of $< n > vs. \kappa$ for all systems in a clean phase diagram. At each point, there is a pairing of $(< n >, \kappa)$ and the color of the point corresponds to how many clean systems share these two parameter values of number density and compressibility.

3.3 Binary Disordered System

Since we know at this point the phases are weakly correlated with one another through the data shown in section 3.2, we should seek to observe what is happening at the local level. Disordered phase diagrams have similar features and have shapes that are dependent on the actual disorder itself. The Bose glass phase appears only with disorder applied across all real systems used in the calculation of the disordered phase diagrams [1,3,11], and it characteristically separates the Mott lobes from the SF region. Recall that Bose glass is characterized by a finite compressibility, zero-SF density and any number density value.

3.3.1 Phase Diagram for System of Binary Disorder

We begin the observance of disorder's effects by looking at a binary (two value) disordered lattice. With binary disorder, only two Hamiltonians are randomly considered at each lattice site and for a system of disorder strength range: $[-\Delta/2, \Delta/2]$, they are:

$$h_{i,1} = -t\left(a_i^\dagger \langle a_j \rangle + \langle a_j^\dagger \rangle a_i\right) + \frac{U}{2} n_i(n_i + 1) + \left(\frac{\Delta}{2} - \mu\right) n_i \qquad (9)$$

Or

$$h_{i,2} = -t\left(a_i^\dagger \langle a_j \rangle + \langle a_j^\dagger \rangle a_i\right) + \frac{U}{2} n_i(n_i + 1) + \left(-\frac{\Delta}{2} - \mu\right) n_i \qquad (9)$$

A system of ternary (three divisions) disorder then will consider a third Hamiltonian, where the disorder potential is $V_i = 0$.

Figure 3.3 shows a binary disordered system phase diagram for compressibility and its respective phase boundary. The phase boundary gives an idea as to where the system goes from zero to finite compressibility. The Bose glass phase is predicted to appear as a separating phase between these lobes and the region of SF systems adjacent to them [1,3].

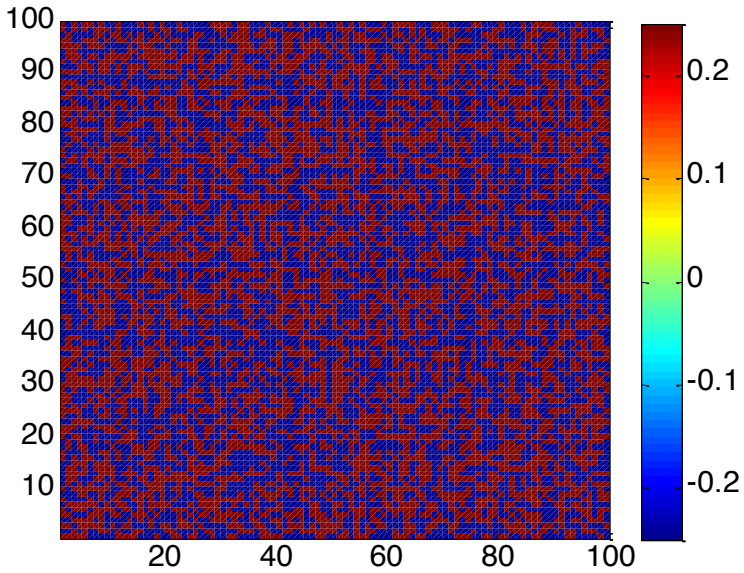

FIG 3.4: A binary disorder map, where each colored square is either adding a potential of 0.25 or -0.25 to the system site it matches up with. This 100 x 100 disorder map can be visualized as an overlay across a real optical lattice with the disorder potentials raising or lowering trap potentials at each site randomly.

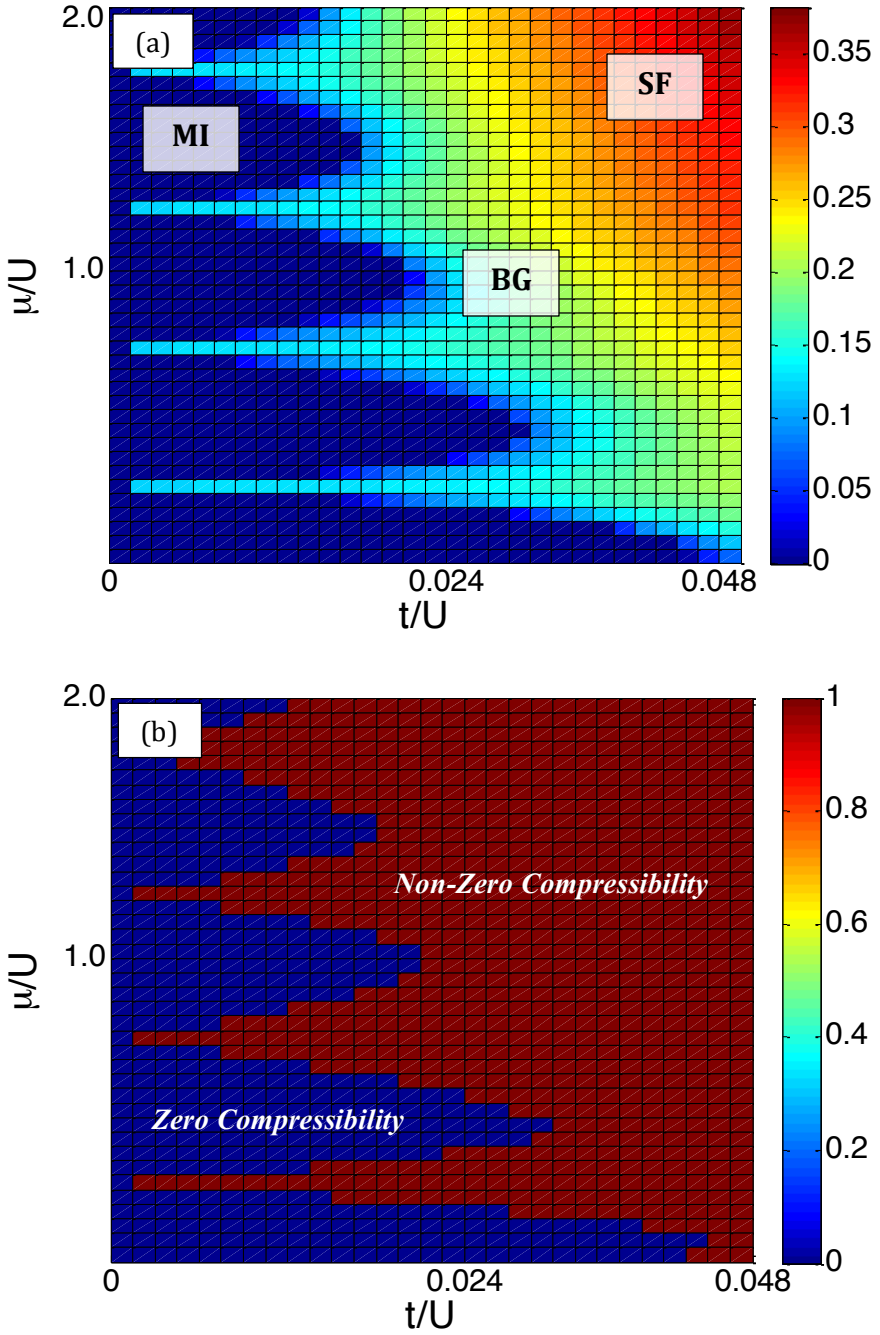

FIG. 3.5 A compressibility phase diagram for a binary disordered system and its correlated phase boundary (i.e. where the system goes from SF to MI). The disorder strength is $\Delta = 0.5$ and since it is binary, there are only two different disorder potentials randomly assigned to each site. The phase boundary plot was done with the conditional C_i referenced above and the disorder map used is in Fig. 2.1.

The binary model has one of two divisions of disorder, and as the strength of the disorder changes – so does the displacement and shape of the Mott lobes. The predicted region of Bose glass arises out of the Mott Lobes, and completely separates the MI from the SF region as long as the disorder strength Δ is less than the site potential ($\Delta < U$). If the disorder is greater than the site potentials, $\Delta > U$, then there is only a region of Bose glass throughout the entire system, and no MI is present [4]. Any system located in this Bose glass region should show no superfluid density and non-zero compressibility and number density. This is apparent when observing the maps showin in Figure 3.6.

3.3.2 Local Phases for Binary Disorder Potentials

Now we need to look at what is happening locally in this expected Bose glass region. To do so, actual lattices must be observed and their phase dependent parameters measured. Figure 3.6 shows the compressibiliy, SF density and number density of three real lattices located at different points in the binary phase diagram identified through their (*t/U, μ/U*) values to show their position. The points were chosen specifically in the MI, Bose glass and SF regions of the binary phase diagram (Figure 3.5). In the first three sub figures at point: (0.012, 0.5) in the phase diagram, there is a uniform zero compressibility, zero SF density and integer number density $n = 1$ which aligns precisely with the characteristics of the MI phase. The second set of three sub figures is at the Bose glass region point: (0.021, 1.0), and is our main topic of interest. We can see that there is a finite SF density and compressibility at some lattice points, but still large pockets of MI present. At every point where there is zero SF density, there is also zero compressibility and integer number density. In contrast, at every point there is finite SF density, there is also finite

compressibility and any number density value. When taking the average of all the parameters' values, we see a finite number density and compressibility, but still there is no superfluid density (only pockets). This observation, coupled with the property that local site phases are weakly correlated with those of neighboring sites, proves that there is no exotic phase arising between the two known clean system states and only a local mixing of MI and SF. When taking the average of all the parameters separately (which is what is done when creating a SF phase diagram) there are mixed phase determining characteristics which would imply the presence of a third phase, but locally there is no such thing. There is simply either MI or supefluid present at each site. We renforce this observation through looking at systems with more complex disorder than binary in sections ahead. In the final three sub figures of Figure 3.6, there are real system parameter plots in a region of SF. Though there is disorder present, the entire system has no MI pockets present and has non-zero superfluid density throughout the entire optical lattice.

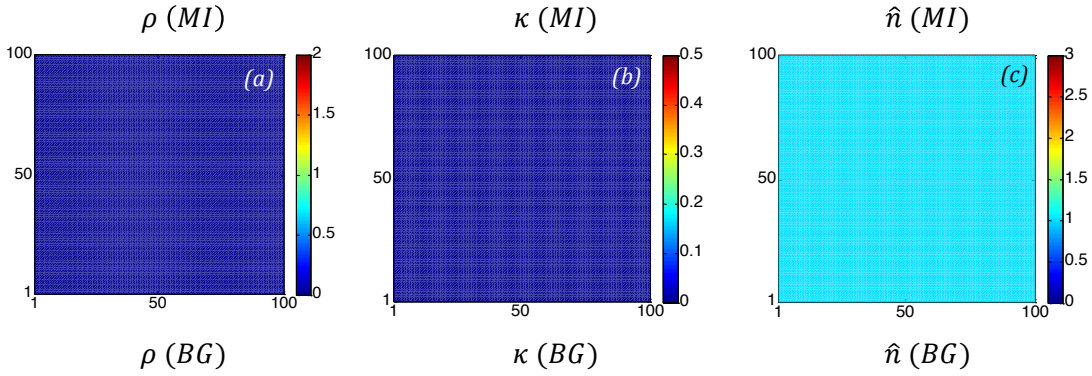

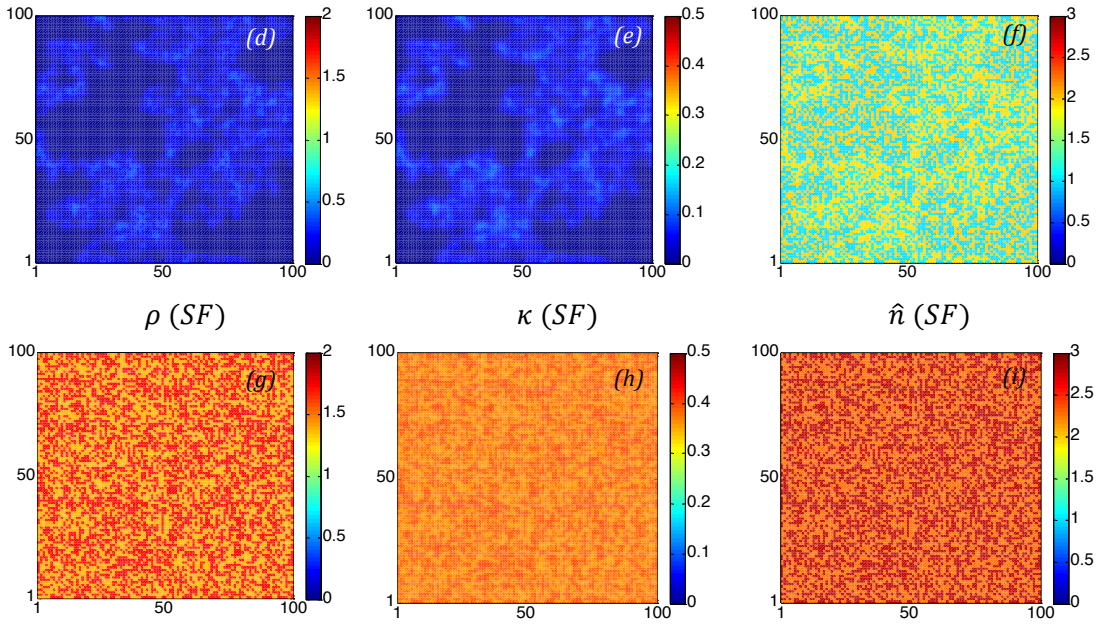

Fig. 3.6: Nine real-space lattice parameter diagrams that are of different points in binary disorder phase space (Figure 3.5). In the first row, we have chosen the point (0.012, 0.5) on the diagram that is located deep within the Mott region. Each site shows a uniform zero SF density, zero compressibility and finite/integer number density. For the second row, we have chosen a point in the Bose glass region of the phase diagram (0.021, 1.0). Notice that there are present SF clusters, but are surrounded by a region of MI (zero compressibility, zero SF density and non-integer number density). For the final row, we have chosen a point that is in a known region of SF: (0.045, 1.95). These systems show a non-uniform finite SF density over every site, finite compressibility and uniformally integer/non-integer number density.

3.4 Ternary Disordered System

To increment the disorder complexity in a small step, we will observe what happens in a ternary disordered system. Recall that with ternary disorders, there is now the consideration of a third Hamiltonian which has a disorder potential $V_i = 0$. A ternary

disorder compressibility phase diagram is shown below in Figure 3.8. In the figure, there are smaller lobes in between the two larger lobes. This is characteristic of disordered lattices, and the amount of smaller intermediary lobes is dependent upon the total amount of possible Hamiltonians solved in the disordered real systems at each square in the diagram. The disorder map used to craft all ternary disordered systems in Figure 3.8 and 3.9 is shown in Figure 3.7.

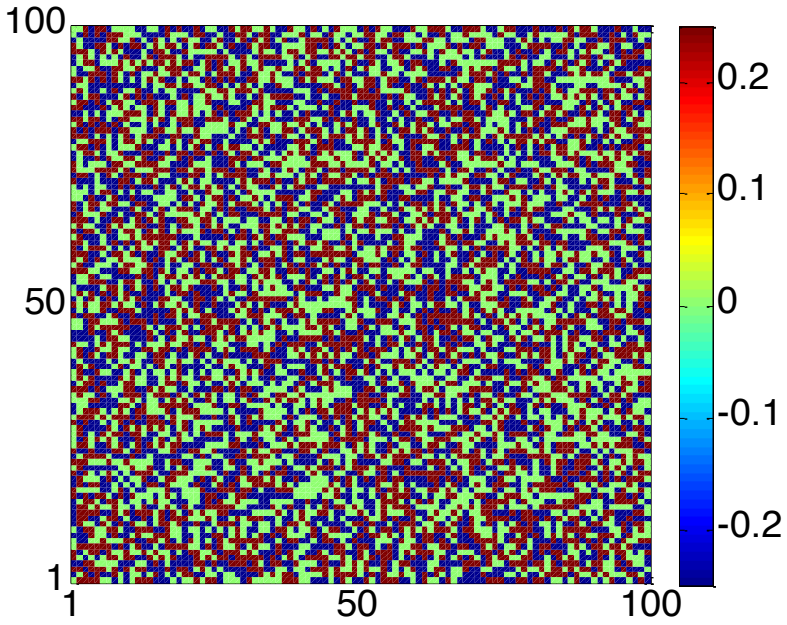

Figure 3.7: A disorder map created for a ternary system. Comparing to the binary disorder map shown in Figure 3.4, there is only a single added disorder potential of $V_i = 0$ scattered randomly across.

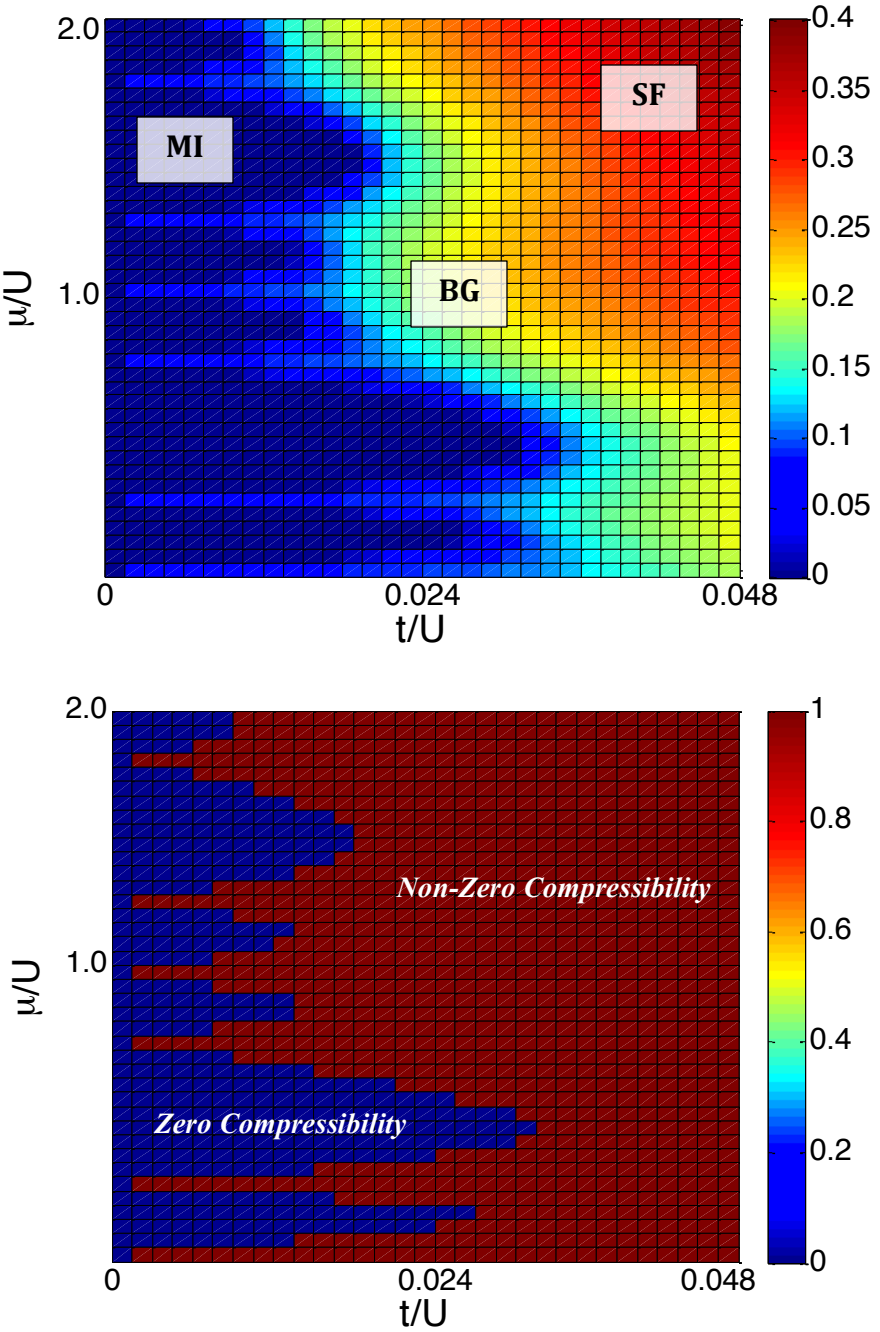

Figure 3.8 A ternary disordered compressibility phase diagram with disorder strength $\Delta = 0.5$ and its phase boundary diagram. Again, an expected region of Bose glass separates the Mott lobes from the SF systems. We utilized the phase boundary algorithm discussed in 2.4 to find the compressibility boundary diagram.

In the next section we observe the real lattices at points chosen in the regions of MI, SF, and Bose glass to further enforce site exclusivity to either the MI or SF phases.

3.4.1 Local Phases for Ternary Disorder

Figure 3.9 shows lattices in the same pattern as what was done with the binary disordered system. The points chosen in ternary disordered phase space (Figure 3.8) are optical lattices in the MI, Bose glass and SF region and are disordered through the disorder map in Figure 3.7.

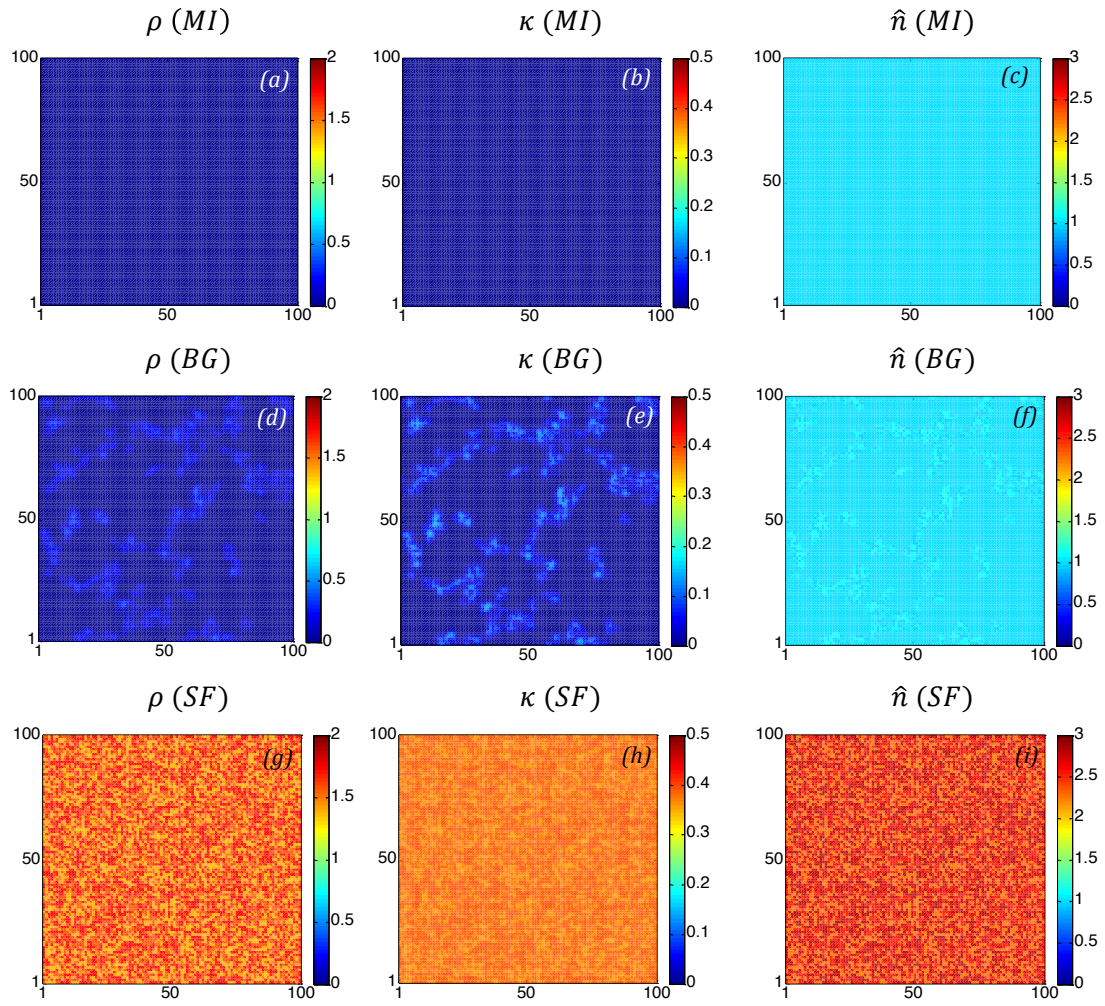

Figure 3.9: The above table shows lattice SF density, compressibility, and number density at three different points on the ternary phase diagram which correspond with the

three different phases. The first row is at site (0.006, 0.5) and gives the characteristics of a MI, where there is zero SF density, zero compressibility and a uniform integer number density. The second row, (0.03, 0.5), gives parameter values in the Bose glass region, and shows the presence of SF clusters (but zero-SF density and compressibility) on a background of MI. The final row, (0.045, 1.95), has finite SF density, finite compressibility, and a integer/non-integer number density across all sites, confirming it is in a SF state.

Through the diagrams shown in Figure 3.9, we can see that there are defined regions of MI and SF in the Bose glass system, with no actual intermiediary phase present. For our final case, a system with large amounts of disorder is considered. And we prove that there is still defined regions of solely SF and MI in the Bose glass area of the phase diagram.

3.5 Complex Disorder Applied Across a System

For the final portion of this chapter, we consider a uniformly disordered system. The 41 different values of disorder potential in a $(-0.25, 0.25)$ strength spectrum are randomly distributed. This is to further solidify our claim that the Bose glass phase does not appear on a local level. Figure 3.11 shows in similar pattern the parameter mappings for real lattices located at different point in the high disorder phase diagram (Figure 3.12). We can see that when overlaying the different paired parameter maps, there is only the MI or SF phases, and no exotic mixture between them (e.g. zero SF density at a compressible site). This shows that for any amount of disorder present, the Bose glass phase is still only present when observing statistical averages of each system parameter.

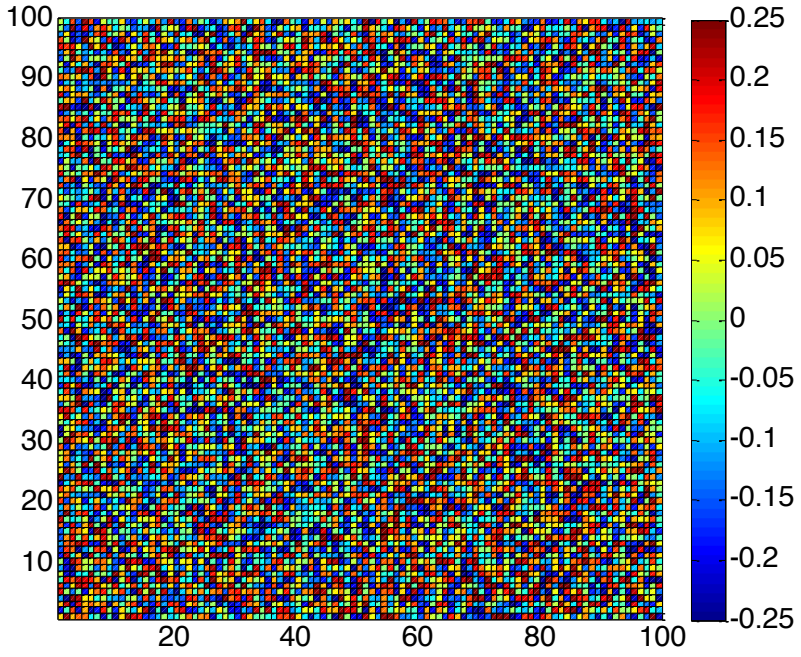

Figure 3.10: A disorder map for 41 divisions of disorder spread across a disorder potential spectrum $\Delta = 0.5$. This is used to disorder systems utilized in Figures 3.11 and 3.12.

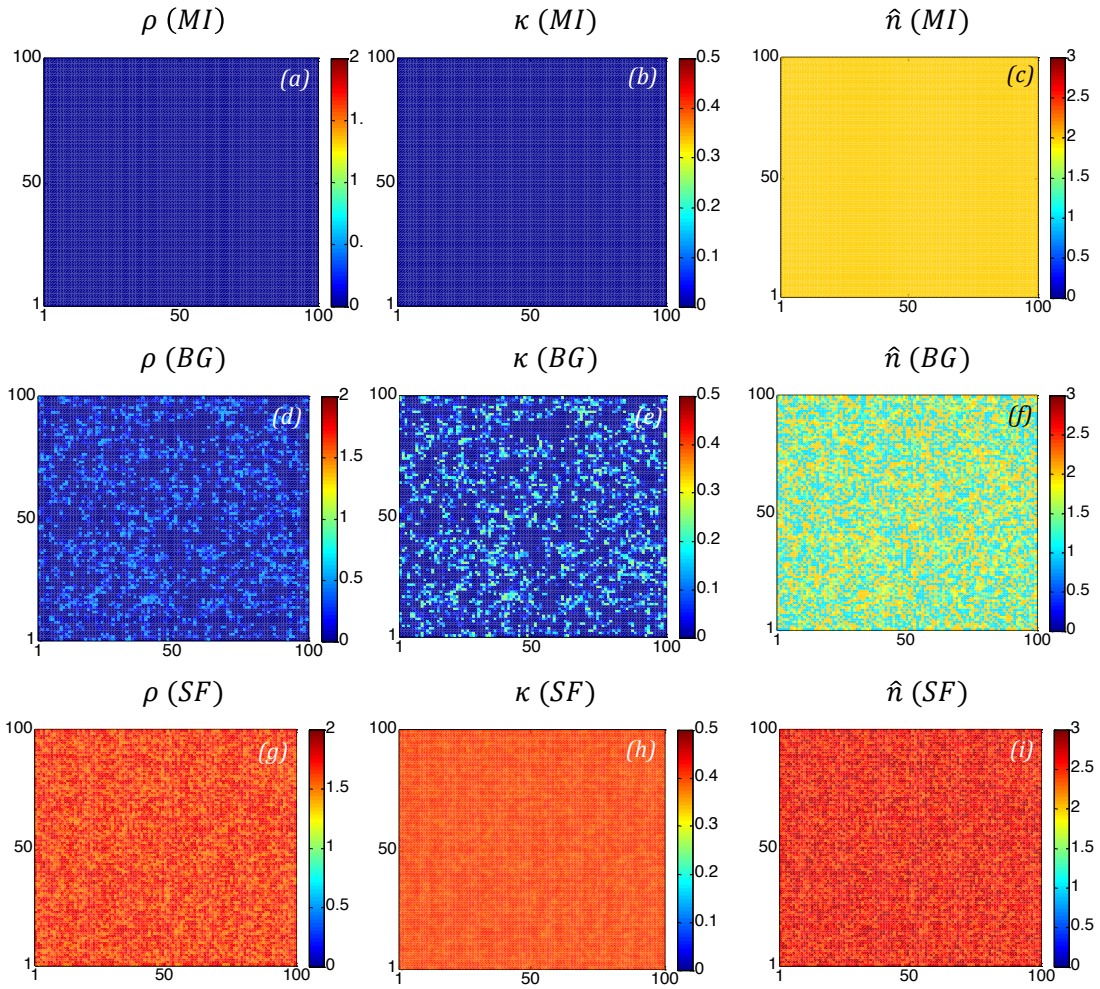

Fig. 3.11: Nine real lattices for parameters SF density, compressibility and number density. The first three sub figures (a, b, c) are at the point (1.5, 0.003) on the disordered phase diagram Figure 3.9. The second three (d, e, f) are located at point (1.0, 0.009) in the Bose glass region of Figure 3.9. The final three (g, h, i) are located at point (1.99, 0.048) in the SF region. Notice that in d, e, and f, there is still the separation of the MI and SF clusters.

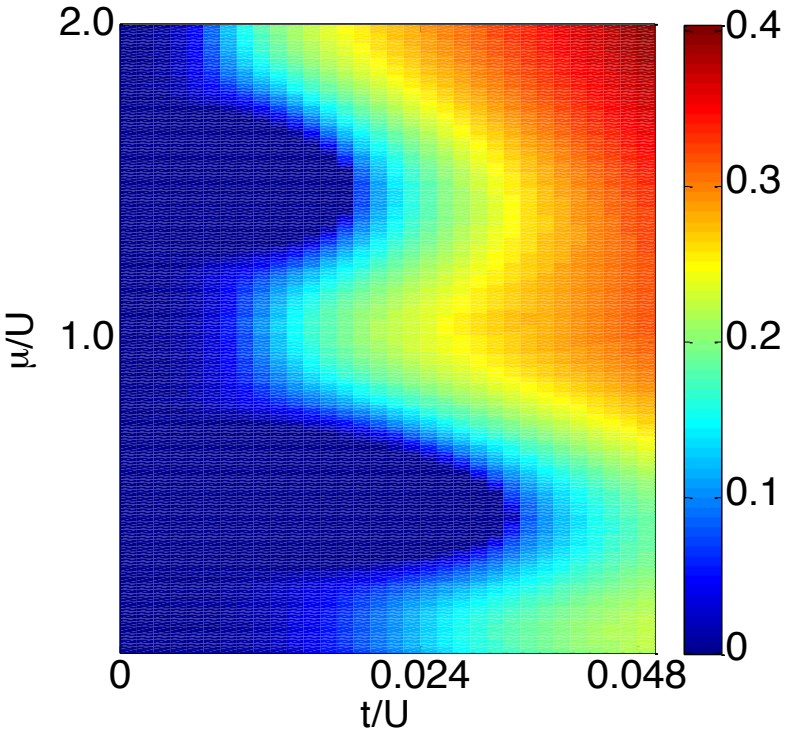

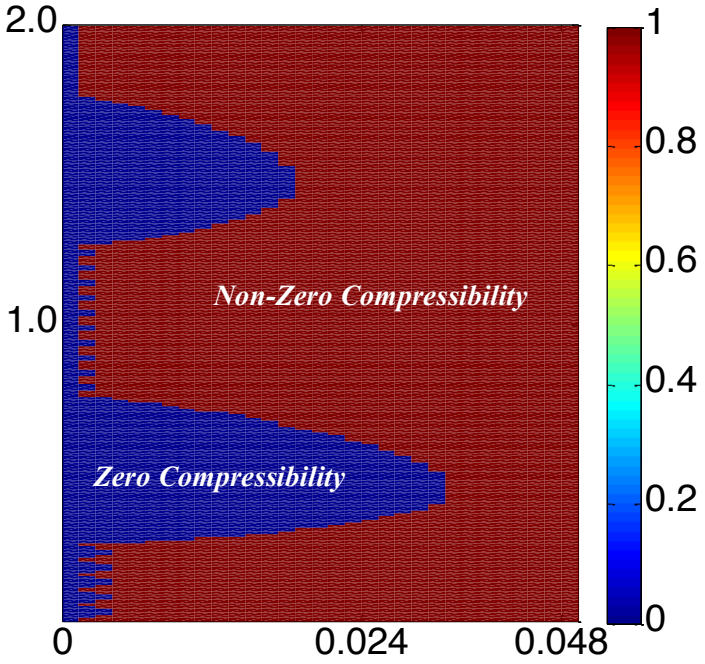

Figure 3.12: A continuous disorder phase diagram created with 41 divisions of disorder potential over a (-0.25, 0.25) potential strength spectrum. The intermediate Mott lobes

have become too small to see, and the Bose glass section is larger between the MI and SF.

From our observation of the (κ, n) relationship between a continuously disordered lattice and multiple clean systems, we have seen that there is a weak phase correlation between sites in the disordered system. Then, since we know there is weak correlation, the observance of actual lattice parameters shows that any site phase is largely dependent upon its local disorder potential. Through these important observations and the real-system lattice diagrams, we have seen there will always be a separation of MI and SF at the local sites. Therefore, the Bose glass is solely present when observing averaged parameter values through phase space, and does not separate the MI and SF phases when observed at the local level.

CHAPTER 4. PREDICTION OF THE DISORDERED PHASE DIAGRAM

Assuming disorder is evenly distributed probabilistically, each site has the even chance of receiving any possible disorder potential. Because of this, we can craft a mechanic that creates all possible shifted clean diagrams and takes the average over all of their phase space values. The shifted diagrams compared to our actual simulated and calculated diagrams are shown in Figure 4.1. In the left-hand column there are the 'shifted' disordered phase diagrams and in the right-hand column, the actual calculated diagrams are displayed (by calculated, we mean created through our simulation mechanic discussed in chapter 2). Through the discovery that the site phases are weakly correlated with one another, we have predicted correctly the disordered phase diagrams using only the knowledge of phases in clean systems.

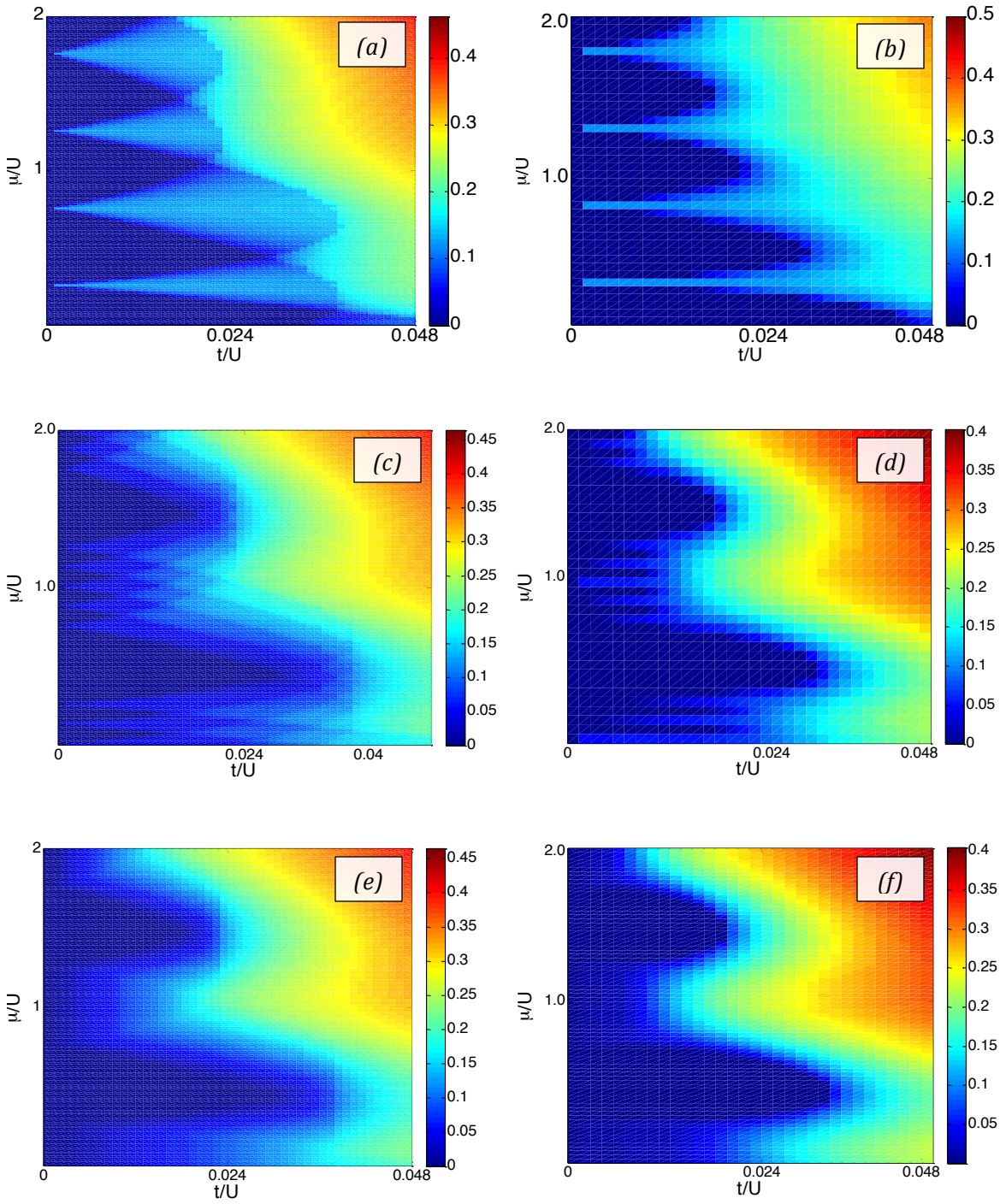

Figure 4.1: The predicted and calculated compressibility phase diagrams of disorder systems. In the left-hand column, the shifted diagrams are displayed. On the right-hand side, the Bose Hubbard Model calculated diagrams are displayed.

CHAPTER 5. CONCLUSION

Experimental observation of the Bose-Einstein condensate was a landmark discovery that fueled many new experiments and discoveries to be built upon its foundation [13]. In this theoretical study, a relationship has been found between clean systems and disordered system sites through pairings of local compressibility and number density. Because of this, each system site in a disordered lattice isn't largely affected by different neighboring site phases. In other words, the quantum phases pertaining to optical lattice sites in a disordered Bose-Einstein condensate are largely independent from one another and dependent solely on the disorder potential placed at each site and local site characteristics. Through the careful analysis of real systems, the theoretically predicted Bose glass phase is apparent only through system-wide parameter averages. When focused solely on single site phases, there is no intermediary Bose glass phase. Since the system sites of a disordered lattice very weakly correlate between one another, an averaging of all shifted clean phase diagrams for every possible disorder potential within a disordered system proved to be a successful disordered phase diagram prediction mechanic.

The consideration of disorder is always important when optical lattices are observed experimentally. The precision and tools used to craft and observe these systems have become very advanced and defined [7], but certain inevitable fluctuations of site potentials could still persist [10,14]. A three-dimensional application utilizing our parameter observations coupled with the approximated Bose-Hubbard model would be a viable option for building off of what we have found.

REFERENCES

1 M. Fisher, G. Grinstein and D. Fisher, Physical Review B 40, (1989).

2 Particleadventure.org, (2014).

3 A. Niederle and H. Rieger, New J. Phys. 15, (2013).

4 L. Fallani, J. Lye, V. Guarrera, C. Fort and M. Inguscio, Phys. Rev. Lett. 98, (2007).

5 M. White, M. Pasienski, D. McKay, S. Zhou, D. Ceperley and B. DeMarco, Phys. Rev. Lett. 102, (2009).

6 J. Lye, L. Fallani, M. Modugno, D. Wiersma, C. Fort and M. Inguscio, Phys. Rev. Lett. 95, (2005).

7 W. Bakr, A. Peng, M. Tai, R. Ma, J. Simon, J. Gillen, S. Folling, L. Pollet and M. Greiner, Science 329, (2010).

8 K. Sheshadri, H. Krishnamurthy, R. Pandit and T. Ramakrishnan, Europhys. Lett. 22, (1993).

9 P. Buonsante, F. Massel, V. Penna and A. Vezzani, Physical Review A 79, (2009).

10 C. Fort, L. Fallani, V. Guarrera, J. Lye, M. Modugno, D. Wiersma and M. Inguscio, Phys. Rev. Lett. 95, (2005).

11 J. Carrasquilla, F. Becca, A. Trombettoni and M. Fabrizio, Physical Review B 81, (2010).

12 M. Greiner, O. Mandel, T. Esslinger, T. Hänsch and I. Bloch, Nature 415, (2002).

13 M. Anderson, J. Ensher, M. Matthews, C. Wieman and E. Cornell, Science 269, (1995).

14 D. Tilahun, R. Duine and A. MacDonald, Physical Review A 84, (2011).